2024 IEEE International Conference on Robotics and Automation (ICRA 2024)
May 13-17, 2024. Yokohama, Japan

LeapRun: A Dynamic Soft Robot with Running and Jumping Capabilities

J. Lu, J. Liang, D. Zhu, D. Wang, Y. Liu, H. Chen, Y. Bai, H. Zhang, and M. Zhang*

***Abstract*— In the natural world, insects exhibit remarkable locomotion capabilities through a combination of running and jumping. However, replicating this versatile locomotion in a soft robot poses technical and design complexities. Here, we propose a dynamic soft robot named LeapRun that possesses agile locomotion and the ability to perform continuous jumping. To achieve this, a prototype soft robot (weight of 300 mg, size of 30 mm $\times$ 15 mm $\times$ 5 mm), composed of piezoelectric thin film, shape memory alloy, magnet-locking mechanism, and corresponding support structures, is fabricated. Experimental results demonstrate a maximum moving speed of 15 cm/s and a maximum jumping height of 8.7 cm. Continuous jumping of steps and crossing of complex rugged surfaces are realized. Besides, integrated with the power source, wireless communication module, and control module, the untethered operation is also presented, showcasing the potential for multiple applications in search and rescue, exploration, and monitoring.**

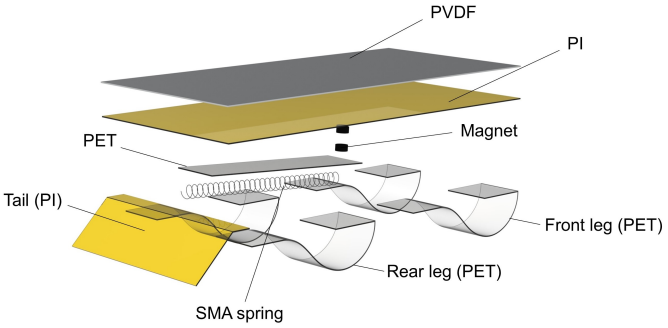

Fig. 1. Exploded view of the soft robot with rapid running and continuous jumping capabilities.

I. Introduction

To escape from predators, broaden the range of activities, and better adapt to complex three-dimensional terrains, numerous insects have evolved rapid moving and continuous leaping abilities [1]. For example, a cockroach can crawl at velocities approaching 60 cm/s even in confined environments [2]; a flea jumping height can exceed 18 cm [3]. The exploration of insect crawling and jumping behavior, coupled with mechanical analysis, can significantly advance our comprehension of the intricate locomotion mechanisms, as well as provide biological inspiration for the engineering design of robots [4], [5].

In recent years, inspired by natural intelligence, significant progress has been achieved in the development of flexible soft robots specializing in both crawling and jumping [6]. Through mimicking the muscles of living creatures, research into crawling soft robots is flourishing with various techniques and materials, including dielectric elastomer actuators (DEAs) [7]–[10], piezoelectric actuators [11]–[13], shape memory alloys (SMAs) [14], [15], ionic electromechanically active polymer (IEAP) [16], reversible thermoresponsive hydrogels [17], magnetic materials [18], ionic polymer–metal composite (IPMC) [19], self-healing electrostatic (HASEL) actuators [20]–[22], and so forth. With respect to jumping robots, based on energy accumulation and rapid release, researchers have integrated specialized actuation mechanisms, such as monolithic three-leaf panel fold structure [23], furcula-like structure [24], bistable von Mises truss [25], ultra-tunable bistable structures [26], torque reversal catapult mechanism [27], two-bars catapult mechanism [28], and more. To notice, certain robots exhibit considerable excellent single-jump performance; however, they encounter limitations in their ability to replicate these jumps continuously [27]–[29]. Therefore, achieving repeatability in dynamic jumping actions is still an existing challenge. Furthermore, designing insect-scale soft robots with multi-locomotion ability that balances both speed and jumping height poses a significant consideration [6].

The movement mechanisms of our bio-inspired objects are detailed here. Cockroaches feature a robust muscular system that endows them with remarkable strength and agility. Notably, their posterior legs boast exceptional development, facilitating rapid propulsion through the coordinated interplay of muscle contractions and relaxations [30]. The fleas' unparalleled leaping ability stems from their extensively evolved jumping legs. When fleas assume a crouched position, their legs and other body components connected via resilient "protein elastin" hinges undergo compression, a state meticulously controlled by muscles. When fleas prepare to leap, their muscles relax, transferring the stored energy from the elastin pads to their legs. This orchestrated leverage action enables the fleas' legs to forcefully strike the ground in a vertical manner, propelling them into impressive jumps [31].

In this work, as illustrated in Fig. 1, we present an insect-scale soft robot (LeapRun) that synthesizes the locomotion strategies observed in both cockroaches and fleas. By harnessing the leverage effect, incorporating piezoelectric material and SMA, the lightweight and compact robot is

This work is financially supported by the Shenzhen Fundamental Research Funds (No. JCYJ20220530143011026).

Jiangfeng Lu, Dekuan Zhu, Dongkai Wang, Ying Liu, Huimin Chen, Yunfei Bai, Haolong Zhang, and Min Zhang are with Shenzhen International Graduate School, Tsinghua University, Shenzhen, 518055, China (corresponding author: zhang.min@sz.tsinghua.edu.cn).

Jiaming Liang is with Tencent Robotics X, Tencent, Shenzhen, 518000, China.

empowered with the ability to crawl and jump. Compared to other single driving principles, the rapid response of piezoelectric materials and the considerable force output of shape memory alloys enable the robot to perform multimodal movements [32], allowing simultaneous running and jumping. This method expands the adaptability of soft robots in complex terrain environments as well as offers fresh insights into the design of agile and multi-locomotion soft robots.

II. Design and Optimization

A. Structure and Working Principle

As depicted in Fig. 1, the prototype robot is composed of a polyvinylidene difluoride/polyimide (PVDF/PI) unimorph actuator, four ring-like polyethylene terephthalate (PET) curved legs, a bifurcation release structure (consisting of SMA, magnets, and PET), and a planar tail. Due to the inverse piezoelectric effect, under the excitation of an external periodic voltage, the main body contracts and extends to drive legs to strike the ground (Fig. 2), generating an undulating gait to mimic the movement of a cockroach [11], [12], [33] (without additional energy-storing for jumping). Our previous research informed the incorporation of a 45° tilting tail to assist in lifting the rear of the body during stair climbing, while the ring-like construction maintains a fixed attack angle of 75° to enhance obstacle negotiation capabilities [34].

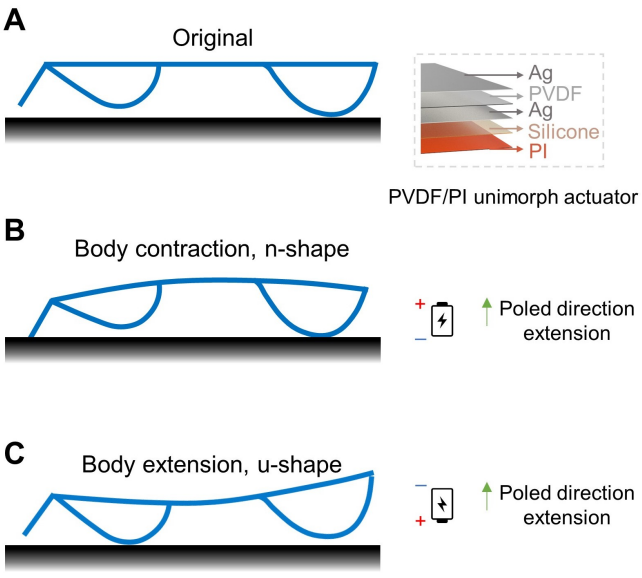

Fig. 2. Actuating principle of the piezoelectric soft robot. Curvature shape under zero (A), positive (B), and negative (C) electric field.

Based on the existing robot structure, Fig. 3 (B) illustrates a bifurcation structure to realize the jumping capability. SMA serves as the driving mechanism, miniature magnets as the lock/release structure, and PET film as the recovery mechanism. The magnetic force F follows Equation (1), and is inversely proportional to the fourth power of the distance x

$$F(x) = \frac{3\mu_0}{2\pi} m_1 m_2 \frac{1}{x^4} \tag{1}$$

where μ_0 is the magnetic permeability, and m_1, m_2 can be calculated through Equation (2)

$$m = MV \tag{2}$$

where M and V refers to the magnetization and volume of the magnets. On the contrary, within a small range of movement, the output force of SMA remains relatively constant. Fig. 4 depicts the correlation between the two torques.

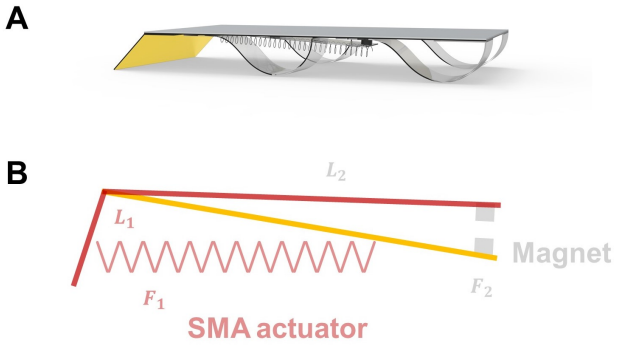

Fig. 3. Insect-scale soft robot with bifurcation leap structure. (A) Model diagram of the robot. (B) Bifurcation release structure.

The leaping process is detailed as follows. Initially, the dominant torque is exerted by the magnetic force. However, as the SMA driver heats up during the locking phase, its output torque gradually increases. Once the SMA torque surpasses the magnetic torque ($F_1 \times L_1 > F_2 \times L_2$), the mechanism is released. Consequently, the magnetic torque rapidly decreases as the rotation angle increases, while the SMA maintains a constant torque output during this stage. At this point, the SMA output torque becomes the primary driving force for the leg's jumping motion.

Then the energy stored in the muscle (SMA actuator) is released abruptly and instantaneously. From the perspective of dynamics, since the force F exerted by the slapping motion is much larger than the support force of the ground and the robot's gravity, according to the impulse-momentum theorem, the initial speed of the robot v_0 can be calculated through the integration of force with respect to time

$$v_0 = \frac{1}{m_r} \int_{t_1}^{t_2} F\,dt \tag{3}$$

where the symbol m_r represents the mass of the robot, while t_1 and t_2 signify the initial and final moments of the impulse, respectively. To achieve a continuous jumping motion, a PET film was affixed to both ends of a pre-stretched one-way SMA spring. As the system was heated, the spring underwent shrinkage, while the elastic potential energy stored in the PET facilitated its restoration to the original state upon cessation of heating. This mechanism enables the system to sustain a seamless jumping motion.

B. Parameter Optimization and Characterization

The performance of the robot is significantly influenced by geometric characteristics. In our previous work [11],

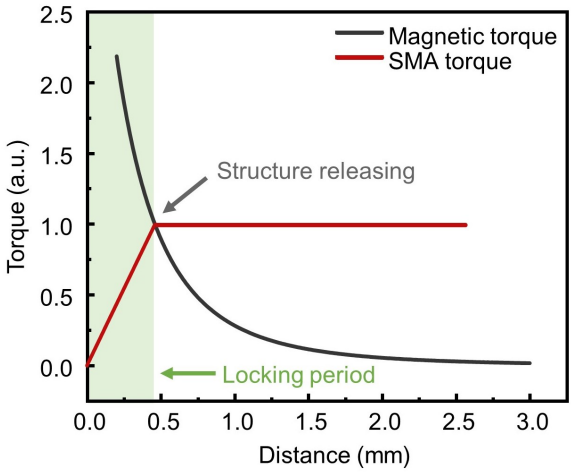

Fig. 4. Magnetic torque and SMA torque variation during the jumping.

[12], [34], we have thoroughly discussed the structure of the actuating part, which plays a crucial role in determining the robot's functionality and capabilities. This section mainly discusses the impacts of magnets, SMA spring, and PET polymer. In general, the stronger the magnetism of the magnet, the greater the force required from the SMA for release, resulting in a more forceful impact on the ground. However, this can also lead to issues such as excessive payload, longer heating and cooling times, and challenges in the recovery process. Therefore, it fundamentally becomes a tradeoff between these factors. We proposed a corresponding metric called "continuous jumping index" k to evaluate the efficiency and coherence of the robot in continuous jumping missions. It can be defined as

$$k = \frac{v_0}{t_r} \tag{4}$$

where v_0 is the initial speed and t_r refers to the recovery interval or cooling time, because the heating time can be adjusted by modifying the current, while heat dissipation is solely achieved through convection with air.

The continuous jumping index could be optimized through the following formulas in the heating and cooling process. Due to the SMA wire diameter is relatively thin, the temperature distribution could be assumed as homogeneous and convective heat transfer coefficient h as constant [35]. The source of heat in this case originated from the Joule heating resulting from the electrical current I applied to the SMA. Then for time variable t, we have

$$\frac{dE_p}{dt} + cm\frac{dT}{dt} = I^2R - hA(T - T_\infty) \tag{5}$$

where E_p, c, m, T, R, A, and T_∞ refer to the stored elastic energy, specific heat capacity, mass, current temperature, resistance, surface area, and surrounding temperature of SMA. For the cooling process, the above equation can be rewritten as

$$cm\frac{dT}{dt} = -hA(T - T_\infty) \tag{6}$$

TABLE I
SPECIFICATIONS OF THE ROBOT

Feature	Value
Robot size (L×W×H)	30 mm × 15 mm × 5 mm
Robot mass	300 mg
Magnet dimension (r×h)	0.5 mm × 1 mm
Spring initial length	10 mm
Spring pre-stretch length	15 mm
SMA wire diameter	0.1 mm
SMA coil diameter	1 mm
PET size (l×w×t)	15 mm × 4 mm × 0.15 mm
Four curved legs (l×w×t)	20 mm × 3.5 mm × 0.1 mm

The same robotic framework is utilized [34], and the previously indicated equations are used in simulation to optimize the SMA, PET, and magnet characteristics. Several attempts and evaluations have been undertaken to experimentally determine the corresponding material parameters. Finally, the following parameters, shown in Table. I, were employed in this work.

C. System Control Simulation

To comprehensively visualize the entire control process, including heating and cooling, we employed MATLAB/Simulink (R2023a, MathWorks Inc.) module for presenting this process. Considering the intricate nature of forces exerted by SMA at varying temperatures, we utilized COMSOL Multiphysics (version 6.1, COMSOL Inc.) simulation calculations to accurately determine these forces. The forces between the magnets were also calculated, and both sets of data were subsequently imported into MATLAB for further analysis and processing. The resulting system block diagram and corresponding outcomes are presented in Fig. 5. Theoretical simulation results indicate a heating time of 0.9 s and a cooling time of 3.1 s, and the energy consumption for a single jump is computed to be 0.83 J. Experimental data is provided in Section III.

III. Results and Discussion

A. Electrical Driving Scheme

The two layers of silver electrodes on the robot's main body are connected to an external electrical driving system by 50-μm-diameter silver wires. These wires are securely attached using 2 mm × 2 mm aluminum tape. The SMA actuator is connected to a 3.7 V direct current (DC) power source, with wires attached to its two terminals. The electrical driving setup is depicted in Fig. 6. The entire system, except for the DC power, comprises a signal generator module, an amplifier module, and the robot itself. A voltage between −2.5 V and +2.5 V from the signal generator is amplified by a factor of 100 before applying on the robot's unimorph actuator.

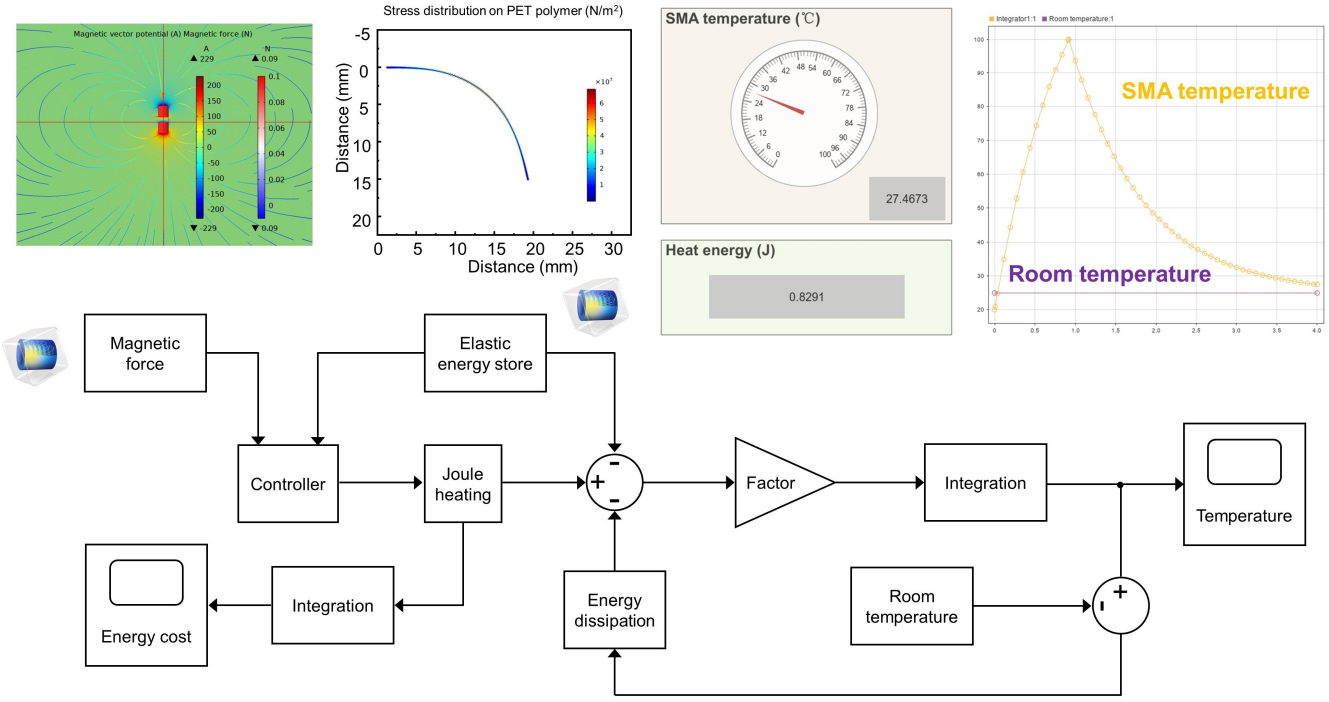

Fig. 5. Integrated visualization of the control process, composed of COMSOL simulation data, heating and cooling processes, and an interactive panel.

B. Continuous Jumping for Traversing Steps

The application of soft robots in continuous jumping, particularly in traversing steps, holds significant potential in various fields and scenarios, including environmental detection in hazardous areas, disaster rescue, and other fields. Compared with their rigid counterpart, soft robots offer adaptability, compliance, impact reduction, enhanced stability, versatile motion, and application diversity [36].

Two steps (individual height of 30 mm, six times of the robot's height) were established for this experiment. The robot was able to achieve bouncing by striking the ground through the SMA actuator. Fig. 7 illustrates that the robot's jumping speed is not entirely vertical. This is due to the PET's bending, which generates an upward slope in the striking speed in the robot's head direction. This phenomenon is in line with the typical insect jumping pattern [37]. In addition to smooth landing, from the experimental results (The experiment of the same robot's locomotion characteristics was repeated ten times and averaged), the heating time, recovery interval, maximum jumping height, and half jumping distance are 1 s, 2.5 s, 8.7 cm, and 4.5 cm, respectively.

During the jumping process, the voltage and current were measured at 3.7 V and 0.3 A respectively, with a heating time of 1 s and an energy consumption of 1.11 J per single jump. Energy-wise, with the utilization of a 40 mAh lithium polymer battery, boasting a voltage rating of 3.7 V (manufactured by HuiXinLi, Inc.), the robot exhibits the ability to execute an impressive 480 consecutive jumps. These findings underscore the high practical potential of the robot for real-world applications.

C. Multi-locomotion for Traversing Rugged Terrains

Given that insects often navigate through environments with complex topography, it becomes crucial to enhance their capability to traverse such terrains [38]. In this section, as shown in Fig. 8, we constructed terrain with slopes (tilting angle of 15°) and plummet terrain (refers to the top of a series of piles). Actuated by alternating voltage (square wave, ±250 V, resonant frequency of 210 Hz), the speed of movement on the flat surface was 15 cm/s. The effect of the bouncing structure on the velocity was not significant, demonstrating the compatibility of crawling and jumping, consistent with our prior research [11], [12]. It is worth noting that the robot exerts less force while striking the ground over rough or soft terrain, resulting in lower jump heights. Nonetheless, this strategic approach holds significant potential in assisting the robot to overcome current limitations related to ground conditions and adjust its posture accordingly.

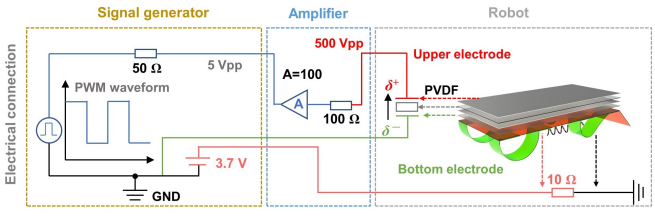

Fig. 6. The electrical driving system utilized for the robot. This comprehensive system comprises three main components: the control signal generator, amplifier, and the robot itself.

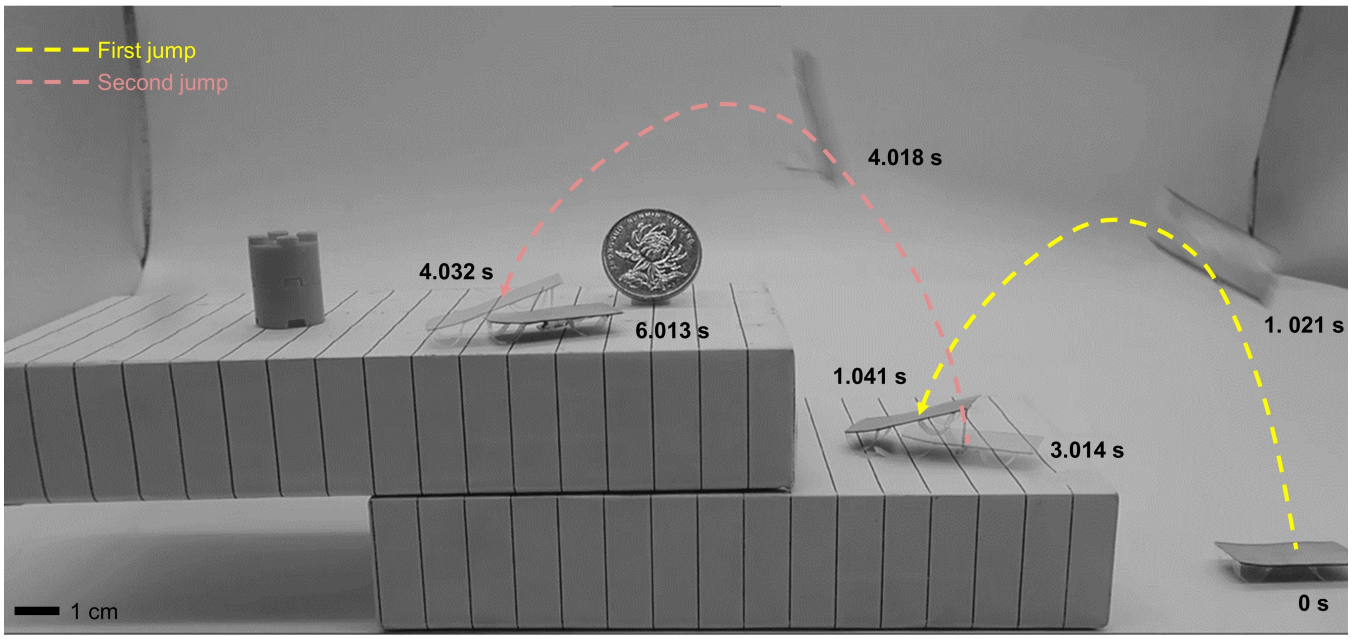

Fig. 7. Continuous jumping for traversing steps with parabolic trajectory. The recovery time for the two jumps were 1.97 s and 1.98 s, respectively.

D. Untethered Operation

To mitigate the constraints imposed by cables on the movement of the soft robot, the same board demonstrated in [12], [39] was utilized on this robot for crawl actuation as well. As shown in Fig. 9, the 1390 mg circuit board was bonded to the robot body through the support beam. In this case, the measured speed of the robot on the flat ground is 1.98 cm/s. For cable-free jumps, an RF transmitter and the corresponding receiver (Fengniao Inc.) were employed to establish wireless serial communication with the robot. This communication setup facilitated remote control of the robot's SMA actuator state, allowing for the precise control of when the actuator is turned on or off by manipulating the AO3416 [14] (20V N-Channel MOSFET, maximum continuous drain current of 6.5 A, Alpha & Omega Semiconductor Co., Ltd.). Then the load was strategically placed at the center of gravity of the robot to prevent from tilting forward or backward during the jumping process. As anticipated, both the jumping height and the distance covered by the robot during half a jump were observed to have decreased to 1 cm and 1.5 cm.

We must declare that the operational speed and jumping capability of the robot are significantly reduced due to the individual battery's mass of 850 mg, which is approximately three times the weight of the robot itself. Additionally, considering the robot's limited load capacity, the next crucial step in our research will involve the ingenious integration of the boost driving circuit and RF control circuit. This will require careful consideration and innovation to overcome the challenges posed by the robot's weight constraints, reduce the battery mass, and enhance its overall performance.

IV. Conclusion and Future Work

In this work, we have introduced LeapRun, a dynamic soft robot capable of agile locomotion and continuous jumping. Building upon the foundation of the original piezoelectric robot, we have implemented SMA, PET, and magnets to enable the robot to perform repetitive jumps by leveraging lever balancing. Importantly, these enhancements do not compromise the inherent locomotion capabilities of the robot. By utilizing simulation, the control process was visualized. Continuous step-jumping capability, traversing rugged terrains, and operating wirelessly were achieved. Through meticulous analysis and refinement, we have validated these abilities, showcasing the potential of the robot in various real-world scenarios.

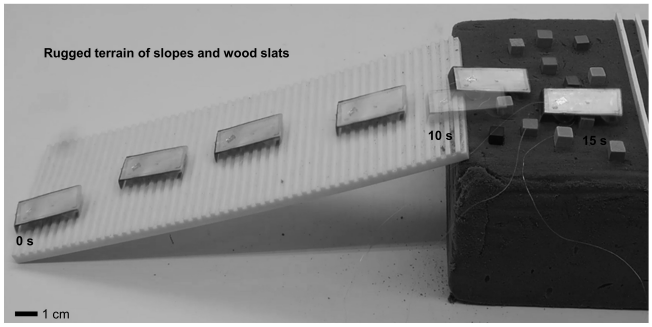

Fig. 8. Multi-locomotion for traversing rugged terrains, including slopes and plummet terrain.

However, we acknowledge that the current design of the robot lacks control over the velocity direction during takeoff, and the inclination angle is susceptible to external load. In addition, the current system lacks a robust steering strategy when navigating through intricate terrains. Moreover, the robot encounters difficulties maintaining a straight-line trajectory, primarily attributed to inherent asymmetry resulting from artificial fabrication.

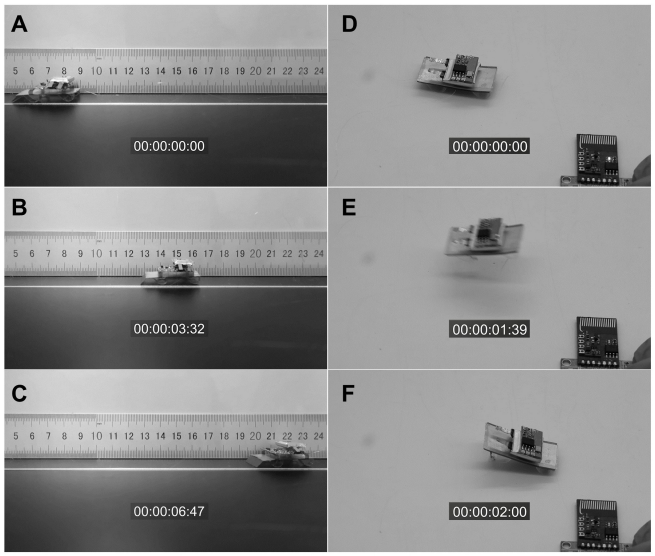

Fig. 9. Untethered operation for the soft robot. (A-C) Movement speed of the robot with a support beam structure loaded with 1390 mg circuit board. (D-F) Jumping process of the robot when equipped with 950 mg load.

Future optimization efforts will be dedicated to achieving precise control over the angle during the robot's ascent, as well as exploring methods to adjust its mid-air posture. Moreover, our future endeavors will prioritize the reduction of cooling time through adaptive methods, thus ensuring the efficient operation of the robot. Furthermore, we will consider incorporating steering structures to enable trajectory control in complex terrains. By addressing these challenges, we aim to enhance the overall performance and versatility of LeapRun, opening possibilities for its application in diverse domains. The pursuit of these objectives contributes to the advancement of soft robot research and facilitates its practical implementation.

V. Material and Methods

A. Main Body Structure Fabrication

By utilizing the slot die coating method, a 28-μm-thick PVDF film (PolyK Technologies, LLC), scaled to 30 mm $\times$ 15 mm, was deposited with 6-μm-thick silver (Ag) film as electrodes on both sides. The sandwiched structure (active layer) was then adhered to PI tape (inactive layer, 120 μm in thickness for polyimide and 25 μm in thickness for the adhesive, Keyun tape Inc.) to generate PVDF/PI unimorph. The exposed tail (15 mm $\times$ 5 mm, tilt angle of 45°) was also fabricated using PI tape. Four curved legs and the membrane in the center that provides the restoring force are all made of PET material (20 mm $\times$ 3.5 mm $\times$ 0.1 mm, 15 mm $\times$ 4 mm $\times$ 0.15 mm, Gizmo Dorks). All the materials were cut using a vinyl cutter (CAMESO 3, Silhouette Inc.). It is worth noting that compared to complex fabrication processes, such as composite structures, the cut-and-fold method provides new insights for future robot designs.

B. SMA Actuator Fabrication

The SMA spring actuator was constructed from an SMA wire (diameter of 0.1 mm, martensitic transformation temperature of 10 °C and an austenite transformation temperature of 60 °C, Hengsheng Inc.). To create a compact spring, the SMA wire was first twisted around a smooth, 1 mm-diameter steel mandrel. Then it is annealed in a tube furnace (OTF-1200X, KJMTI) for 30 minutes at 450 °C [40]. The compact spring was trimmed to 10 mm and stretched to a 15 mm incompact spring that could withstand a 40 % actuation strain after cooling and removing the mandrel. The terminals of the SMA spring are connected to the terminals of the PET membrane, considering the fact that the austenite transformation temperature of SMA is considerably lower than the melting temperature of PET, which is 265 °C. Consequently, the activation process of the SMA actuator has negligible influence on the structural integrity of PET.

In addition, two commercially available strong rubidium iron boron magnets, surface-plated with nickel and zinc, were chosen as locking devices (maximum magnetic force of 150 mN, N35, Xingchuang Inc.). All components were carefully and securely assembled using 502 adhesives (Loctite, Henkel Corporation).

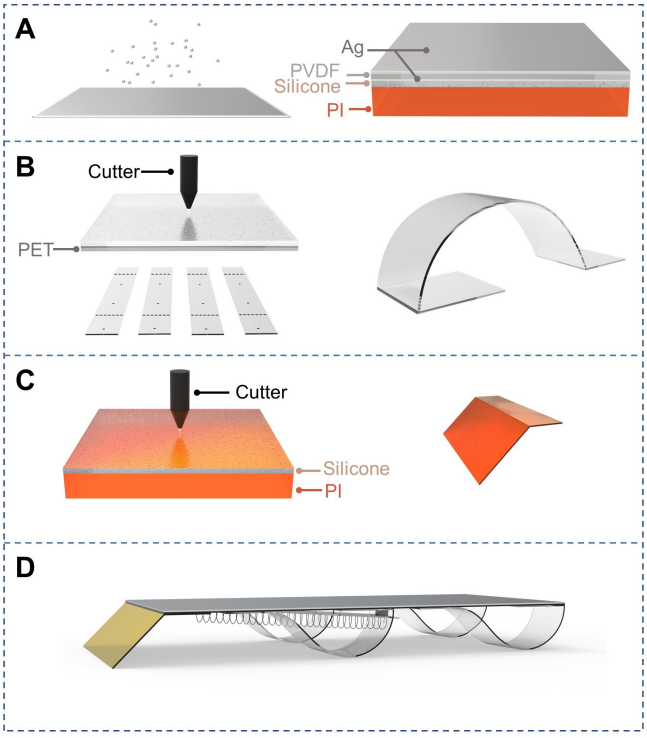

Fig. 10. Diagram of the robot manufacturating process. (A) Depositing silver electrode on PVDF and assembling the robot body. (B) Cutting the robot leg and controlling its curve. (C) Cutting and folding the tail of the robot. (D) Assembling all the components.

REFERENCES

[1] D. Grimaldi and M. Engel, "Evolution of the insects: Cambridge university press, cambridge, 2005," *Journal of Insect Conservation*, vol. 11, no. 2, pp. 211–212, 2007.

[2] K. Jayaram and R. J. Full, "Cockroaches traverse crevices, crawl rapidly in confined spaces, and inspire a soft, legged robot," *Proceedings of the National Academy of Sciences*, vol. 113, no. 8, pp. E950–E957, 2016.

[3] R. Yun, Z. Liu, J. Leng, J. Huang, Y. Cui, X. Yan, and M. Qi, "A 3.4-millimeter flea-sized robot with powerful jumping and fast crawling locomotion," *IEEE Robotics and Automation Letters*, vol. 8, no. 5, pp. 2868–2873, 2023.

[4] M. Ilami, H. Bagheri, R. Ahmed, E. O. Skowronek, and H. Marvi, "Materials, actuators, and sensors for soft bioinspired robots," *Advanced Materials*, vol. 33, no. 19, p. 2003139, 2021.

[5] J. Qiu, A. Ji, K. Zhu, Q. Han, W. Wang, Q. Qi, and G. Chen, "A gecko-inspired robot with a flexible spine driven by shape memory alloy springs," *Soft Robotics*, 2023.

[6] Z. Zhakypov, K. Mori, K. Hosoda, and J. Paik, "Designing minimal and scalable insect-inspired multi-locomotion millirobots," *Nature*, vol. 571, no. 7765, pp. 381–386, 2019.

[7] G. Gu, J. Zou, R. Zhao, X. Zhao, and X. Zhu, "Soft wall-climbing robots," *Science Robotics*, vol. 3, no. 25, p. eaat2874, 2018.

[8] C. Tang, B. Du, S. Jiang, Q. Shao, X. Dong, X.-J. Liu, and H. Zhao, "A pipeline inspection robot for navigating tubular environments in the sub-centimeter scale," *Science Robotics*, vol. 7, no. 66, p. eabm8597, 2022.

[9] X. Ji, X. Liu, V. Cacucciolo, M. Imboden, Y. Civet, A. El Haitami, S. Cantin, Y. Perriard, and H. Shea, "An autonomous untethered fast soft robotic insect driven by low-voltage dielectric elastomer actuators," *Science Robotics*, vol. 4, no. 37, p. eaaz6451, 2019.

[10] Y. Liu, B. Chen, W. Li, L. Zu, W. Tang, and Z. L. Wang, "Bioinspired triboelectric soft robot driven by mechanical energy," *Advanced Functional Materials*, vol. 31, no. 38, p. 2104770, 2021.

[11] Y. Wu, J. K. Yim, J. Liang, Z. Shao, M. Qi, J. Zhong, Z. Luo, X. Yan, M. Zhang, X. Wang, *et al.*, "Insect-scale fast moving and ultrarobust soft robot," *Science robotics*, vol. 4, no. 32, p. eaax1594, 2019.

[12] J. Liang, Y. Wu, J. K. Yim, H. Chen, Z. Miao, H. Liu, Y. Liu, Y. Liu, D. Wang, W. Qiu, *et al.*, "Electrostatic footpads enable agile insect-scale soft robots with trajectory control," *Science Robotics*, vol. 6, no. 55, p. eabe7906, 2021.

[13] H. Cui, D. Yao, R. Hensleigh, H. Lu, A. Calderon, Z. Xu, S. Davaria, Z. Wang, P. Mercier, P. Tarazaga, *et al.*, "Design and printing of proprioceptive three-dimensional architected robotic metamaterials," *Science*, vol. 376, no. 6599, pp. 1287–1293, 2022.

[14] X. Huang, K. Kumar, M. K. Jawed, A. M. Nasab, Z. Ye, W. Shan, and C. Majidi, "Chasing biomimetic locomotion speeds: Creating untethered soft robots with shape memory alloy actuators," *Science Robotics*, vol. 3, no. 25, p. eaau7557, 2018.

[15] W. Wang, J.-Y. Lee, H. Rodrigue, S.-H. Song, W.-S. Chu, and S.-H. Ahn, "Locomotion of inchworm-inspired robot made of smart soft composite (ssc)," *Bioinspiration & biomimetics*, vol. 9, no. 4, p. 046006, 2014.

[16] I. Must, F. Kaasik, I. Põldsalu, L. Mihkels, U. Johanson, A. Punning, and A. Aabloo, "Ionic and capacitive artificial muscle for biomimetic soft robotics," *Advanced Engineering Materials*, vol. 17, no. 1, pp. 84–94, 2015.

[17] A. Pantula, B. Datta, Y. Shi, M. Wang, J. Liu, S. Deng, N. J. Cowan, T. D. Nguyen, and D. H. Gracias, "Untethered unidirectionally crawling gels driven by asymmetry in contact forces," *Science Robotics*, vol. 7, no. 73, p. eadd2903, 2022.

[18] Q. Ze, S. Wu, J. Nishikawa, J. Dai, Y. Sun, S. Leanza, C. Zemelka, L. S. Novelino, G. H. Paulino, and R. R. Zhao, "Soft robotic origami crawler," *Science advances*, vol. 8, no. 13, p. eabm7834, 2022.

[19] N. Hu, B. Li, R. Bai, K. Xie, and G. Chen, "A torsion-bending antagonistic bistable actuator enables untethered crawling and swimming of miniature robots," *Research*, vol. 6, p. 0116, 2023.

[20] R. Chen, Z. Yuan, J. Guo, L. Bai, X. Zhu, F. Liu, H. Pu, L. Xin, Y. Peng, J. Luo, *et al.*, "Legless soft robots capable of rapid, continuous, and steered jumping," *Nature Communications*, vol. 12, no. 1, p. 7028, 2021.

[21] E. Acome, S. K. Mitchell, T. Morrissey, M. Emmett, C. Benjamin, M. King, M. Radakovitz, and C. Keplinger, "Hydraulically amplified self-healing electrostatic actuators with muscle-like performance," *Science*, vol. 359, no. 6371, pp. 61–65, 2018.

[22] N. Kellaris, V. Gopaluni Venkata, G. M. Smith, S. K. Mitchell, and C. Keplinger, "Peano-hasel actuators: Muscle-mimetic, electrohydraulic transducers that linearly contract on activation," *Science Robotics*, vol. 3, no. 14, p. eaar3276, 2018.

[23] J. Hu, Z. Nie, M. Wang, Z. Liu, S. Huang, and H. Yang, "Springtail-inspired light-driven soft jumping robots based on liquid crystal elastomers with monolithic three-leaf panel fold structure," *Angewandte Chemie International Edition*, vol. 62, no. 9, p. e202218227, 2023.

[24] V. M. Ortega-Jimenez, E. J. Challita, B. Kim, H. Ko, M. Gwon, J.-S. Koh, and M. S. Bhamla, "Directional takeoff, aerial righting, and adhesion landing of semiaquatic springtails," *Proceedings of the National Academy of Sciences*, vol. 119, no. 46, p. e2211283119, 2022.

[25] Y. Wang, Q. Wang, M. Liu, Y. Qin, L. Cheng, O. Bolmin, M. Alleyne, A. Wissa, R. H. Baughman, D. Vella, *et al.*, "Insect-scale jumping robots enabled by a dynamic buckling cascade," *Proceedings of the National Academy of Sciences*, vol. 120, no. 5, p. e2210651120, 2023.

[26] Y. Jiang, Y. Li, K. Liu, H. Zhang, X. Tong, D. Chen, L. Wang, and J. Paik, "Ultra-tunable bistable structures for universal robotic applications," *Cell Reports Physical Science*, vol. 4, no. 5, 2023.

[27] J.-S. Koh, E. Yang, G.-P. Jung, S.-P. Jung, J. H. Son, S.-I. Lee, P. G. Jablonski, R. J. Wood, H.-Y. Kim, and K.-J. Cho, "Jumping on water: Surface tension–dominated jumping of water striders and robotic insects," *Science*, vol. 349, no. 6247, pp. 517–521, 2015.

[28] H. Chen, J. Liang, Z. Miao, G. Zhou, Y. Liu, and M. Zhang, "Elevation control of a soft jumping robot," in *2021 IEEE International Conference on Robotics and Automation (ICRA)*, pp. 11843–11849, IEEE, 2021.

[29] D. Wang, F. Sui, W. Qiu, Y. Peng, M. Zhang, X. Wang, and L. Lin, "An untethered crawling and jumping micro-robot," in *2021 21st International Conference on Solid-State Sensors, Actuators and Microsystems (Transducers)*, pp. 353–356, IEEE, 2021.

[30] P. Ramdya, R. Thandiackal, R. Cherney, T. Asselborn, R. Benton, A. J. Ijspeert, and D. Floreano, "Climbing favours the tripod gait over alternative faster insect gaits," *Nature communications*, vol. 8, no. 1, p. 14494, 2017.

[31] M. Noh, S.-W. Kim, S. An, J.-S. Koh, and K.-J. Cho, "Flea-inspired catapult mechanism for miniature jumping robots," *IEEE transactions on robotics*, vol. 28, no. 5, pp. 1007–1018, 2012.

[32] L. Hines, K. Petersen, G. Z. Lum, and M. Sitti, "Soft actuators for small-scale robotics," *Advanced materials*, vol. 29, no. 13, p. 1603483, 2017.

[33] Y. Wu, K. Y. Ho, K. Kariya, R. Xu, W. Cai, J. Zhong, Y. Ma, M. Zhang, X. Wang, and L. Lin, "Pre-curved pvdf/pi unimorph structures for biomimic soft crawling actuators," in *2018 IEEE Micro Electro Mechanical Systems (MEMS)*, pp. 581–584, IEEE, 2018.

[34] Y. Liu, J. Liang, J. Lu, H. Chen, Z. Miao, D. Wang, X. Wang, and M. Zhang, "Complex three-dimensional terrains traversal of insect-scale soft robot," *Soft Robotics*, vol. 10, no. 3, pp. 612–623, 2023.

[35] X. An, Y. Cui, H. Sun, Q. Shao, and H. Zhao, "Active-cooling-in-the-loop controller design and implementation for an sma-driven soft robotic tentacle," *IEEE Transactions on Robotics*, 2023.

[36] D. Rus and M. T. Tolley, "Design, fabrication and control of soft robots," *Nature*, vol. 521, no. 7553, pp. 467–475, 2015.

[37] T. Libby, T. Y. Moore, E. Chang-Siu, D. Li, D. J. Cohen, A. Jusufi, and R. J. Full, "Tail-assisted pitch control in lizards, robots and dinosaurs," *Nature*, vol. 481, no. 7380, pp. 181–184, 2012.

[38] H. Marvi, C. Gong, N. Gravish, H. Astley, M. Travers, R. L. Hatton, J. R. Mendelson III, H. Choset, D. L. Hu, and D. I. Goldman, "Sidewinding with minimal slip: Snake and robot ascent of sandy slopes," *Science*, vol. 346, no. 6206, pp. 224–229, 2014.

[39] Z. Miao, J. Liang, H. Chen, J. Lu, X. Sun, Y. Liu, F. Tang, and M. Zhang, "Power autonomy and agility control of an untethered insect-scale soft robot," *Soft Robotics*, 2023.

[40] W. Hu, G. Z. Lum, M. Mastrangeli, and M. Sitti, "Small-scale soft-bodied robot with multimodal locomotion," *Nature*, vol. 554, no. 7690, pp. 81–85, 2018.